Journal of Energetic Materials
Publication details, including instructions for authors and subscription information:
http://www.informaworld.com/smpp/title~content=t713770432

Propellant properties conducive to electrostatic discharge ignition

A. M. Mellor[a]; P. J. Baker[b]
[a] Vanderbilt University, Nashville, Tennessee [b] University of Dayton Research Institute, Dayton, Ohio

To cite this Article Mellor, A. M. and Baker, P. J.(1994) 'Propellant properties conducive to electrostatic discharge ignition', Journal of Energetic Materials, 12: 1, 1 — 62
To link to this Article: DOI: 10.1080/07370659408019338
URL: http://dx.doi.org/10.1080/07370659408019338

PROPELLANT PROPERTIES CONDUCIVE TO ELECTROSTATIC DISCHARGE IGNITION

A.M. Mellor, Vanderbilt University, Nashville, Tennessee 37235
P.J. Baker, University of Dayton Research Institute, Dayton, Ohio 45469

ABSTRACT

A mechanism for electrostatic discharge (ESD) ignition of composite rocket propellants was developed based on review of recent literature on spark–induced ignition of gaseous fuel/air mixtures, dispersions of liquid fuel droplets in air, and solid energetic materials. Ignition implies substantial amounts of available propellant are consumed subsequently. The role of mechanical properties in facilitating ignition by maintaining subsurface hot spot pressure developed by the discharge and products of reaction was identified. Other analysis demonstrated additional thermophysical, thermo–chemical, chemical kinetics, and electrical propellant properties important to ESD sensitivity. Properties which facilitate ignition (e.g., low activation energy for ignition delay) and high propellant burn rate (e.g., small median diameter of oxidizer particle size distribution) favor combustion of the energetic material after a discharge, as do those which inhibit heat losses (small propellant thermal diffusivity) and mechanical deformation or cracking of propellant surrounding the chemically reacting hot spot. Electrical property values which promote breakdown (e.g., high percolation

Journal of Energetic Materials Vol. 12, 1-62 (1994)
Published in 1994 by Dowden, Brodman & Devine, Inc.

coefficient) and substantial deposition of energy in the propellant after breakdown are also discussed.

INTRODUCTION

Spark ignition studies in homogeneous gas mixtures, fuel spray/air mixtures, and energetic materials provide insight into mechanism(s) for electrostatic–induced ignition of solid rocket propellants. Literature from the last ten years received emphasis, in terms of experimental results, engineering models, and detailed computational models, and thus findings of Mellor et al. [1] are updated. Throughout the following, ignition, by definition followed by self–sufficient combustion and substantial burning of the propellant specimen, is distinguished from initiation, which means some reaction (i.e., cracking, popping, appearance of light and/or smoke, etc.) of the propellant to a discharge, not necessarily followed by flame development and propagation. Propellant mechanical failure relates indirectly to sustained combustion since an increase in propellant stress over some critical value causes yielding and/or fracture. Both failure modes lead to reduced and possible quenching, although the latter may actually enhance combustion through increased burning area if cracks do not reach a free surface.

The mechanism for ESD ignition in practical scenarios, developed here, is an outgrowth of one presented by Baker et al. [2] at the 1991 Army Research Office Workshop on Propellant Ignition Micromechanics and is based on the other presentations and discussions at the Workshop, notably

presentations by Wiegand [3] on mechanical failure mechanisms as a function of confinement, and by Isom and Speed [4] on ESD breakdown and ignition. Three flowpaths leading from electrical energy input to initiation, defined as the onset of local chemical reaction, which is followed by either quenching of this reaction or ignition, were identified in the literature by Baker et al. [2] and are compared in Fig. 1. Both Larson and Beale [5] and Isom [6] attribute initiation to microarcs between neighboring metal particles, or local breakdowns through binder. For cases in which oxidizer is available in the vicinity, then chemical reaction between binder and oxidizer can be initiated. If specimen confinement is insufficient [5] or if the high pressure products of reaction formed in the hot spot crack the specimen [6], then hot spots do not grow and coalesce sufficiently to overcome local heat losses to virgin material in the ambient, and they extinguish. With sufficient confinement and cracking suppressed, hot spots reinforce each other leading to ignition and subsequent essentially complete combustion of macroscopic portions of the energetic material sample.

Detailed observations of both large propellant specimens subjected to multiple sparks in the French test methodology [7] and thin, transparent "ant farm" samples led Isom and Speed [4] to a different hot spot mechanism. Instead of microarcs, which deposit very small amounts of energy locally (see also [8]), these workers postulated that continuous breakdown through the binder creates the hot binder decomposition products. Because current flow during the arc following breakdown is not limited to a region between adjacent metal particles, as in the microarc

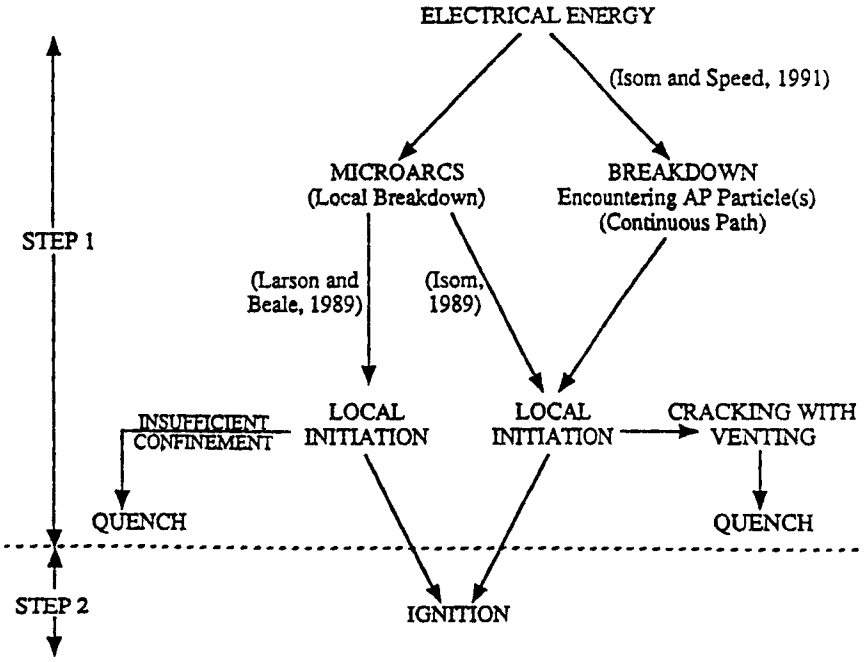

FIGURE 1

Literature pathways for absorption of electrostatic–discharge electrical energy by a solid energetic material [5, 6, 4]. Probability of ignition depends on degree of confinement [2].

resistance to flow of current, both before and after the discharge (surface and volume resistivities). Field amplification effects and the probability of AP positioned near the location(s) of the breakdown also depend on propellant thermochemistry (through its composition and stoichiometry) – a combined thermochemical/electrical property is the percolation coefficient (see for example [15]) that is computed from binder resistivity, metal and oxidizer particle sizes and concentrations, etc.

Finally, mechanical properties play their role as pressure builds up in the hot spot(s) due to the onset of chemical reaction. In line ten of Fig. 4, depending on the pressure and its rise rate and competition between yield and fracture limits of the material, cracks reaching the propellant surface, capable of quenching the reaction, may form. Such issues have been discussed by Baker and Mellor [10], who present an analysis concerned with mechanical response to a chemically reacting hot spot.

Present experiments on and theoretical models for electrostatic discharge ignition of solid propellants are in their formulative stages. Therefore, the spark ignition literature for premixed gaseous and liquid fuel spray–air mixtures was examined for potential applicability to ignition by electrostatic discharge for solid propellants. The case of premixed gases is analogous to homogeneous propellants, while a dispersion of fuel drops in air resembles a composite propellant. The review is largely restricted to quiescent gas or fuel spray/air mixtures, that is, cases for which no velocity relative to the spark electrodes is present. It is felt that this situation is more relevant to the solid propellant case than that with a bulk gas motion. The review is also

theory, substantially more energy can be deposited in the specimen. As before, chemical reaction is initiated if the binder decomposition products encounter nearby oxidizer particles, and hot spots quench or ignite following the balance of the mechanism originally postulated by Isom [6].

Baker et al. [2] suggested two additional quenching mechanisms other than venting of product gases through macroscopic cracks to the specimen surface: for short duration stimuli with high initial rates of current flow, shocks formed as breakdown occurs can transfer thermal energy to propellant outside of the breakdown channel; for long durations, conduction heat losses to neighboring propellant compete with energy release by the chemical reactions. Hodges et al. [9] model only the latter mechanism in their analysis of threshold ESD ignition energy, and they ignore hot spot expansion from the high pressure and the subsequent propellant stress relief [10]. Baker et al. [2] suggest that conduction heat transfer is negligible for durations less than 100 μs, and Maly and Vogel [11] note for spark ignition of gaseous mixtures that short durations relevant to the shock dissipation mechanism are considered 0.1 μs and less.

The ESD mechanism proposed by Mellor et al. [12] is shown in Fig. 2. The pathway by which hot spots form follows that of Isom and Speed [4], except that microarcs are shown as precursors to continuous path breakdown, following Budenstein [13]. The result of hot spot formation varies with confinement, with ignition and combustion more likely at high values.

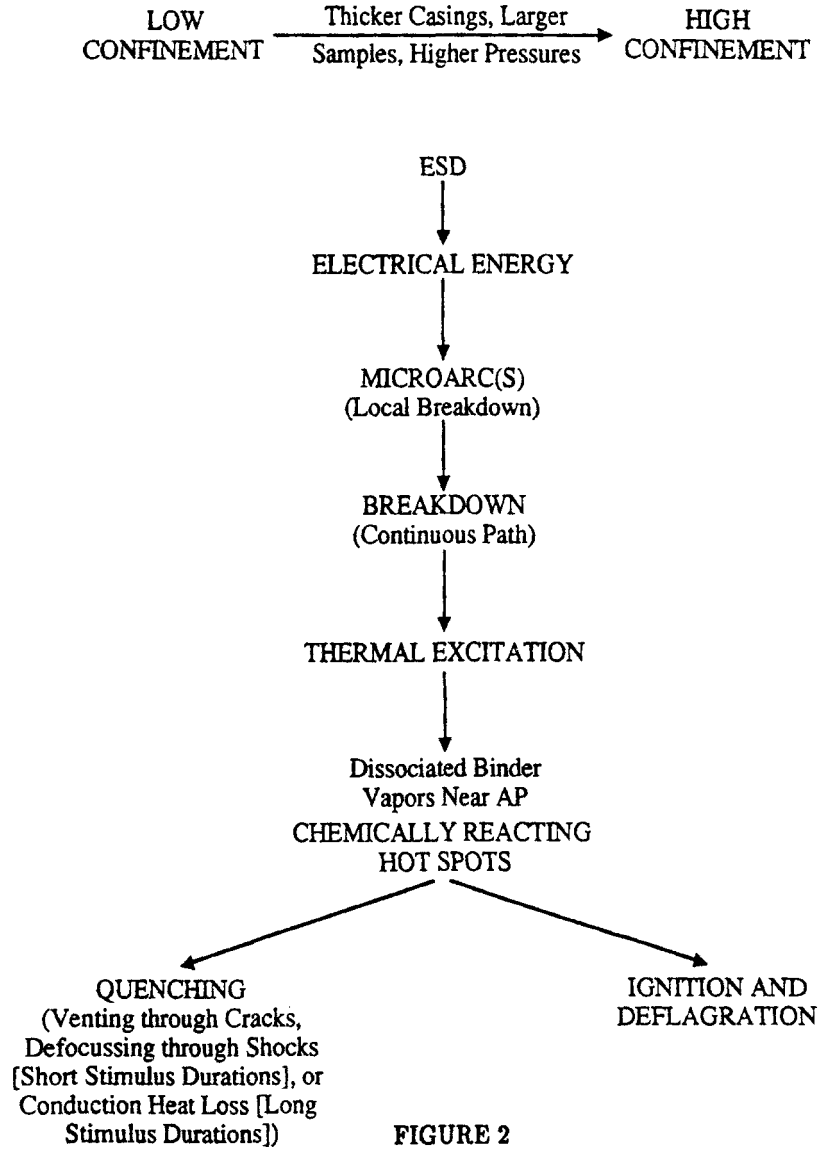

FIGURE 2

Pathways for absorption of electrostatic–discharge electrical energy by a solid energetic material. Failure mechanism and probability of ignition depend on degree of confinement; if chemical reaction extinguishes, then quenching mechanism depends on duration of stimulus [12].

Alternatively, a given level of energy stimulus is more likely to result in ignition as specimen confinement is increased. Hodges et al. [9] have shown this trend with ambient pressure for several propellants, as shown in Fig. 3. The three quenching mechanisms identified by Baker et al. [2] are also retained by Mellor et al. [12], and they become more probable as confinement is decreased.

MECHANISM FOR PRACTICAL SCENARIOS

The flowchart developed by Mellor et al. [12] and shown in Fig. 2 emphasizes events following the first breakdown in a microarc. Both quenching and ignition are shown as the two possible outcomes. However, in manufacturing and fielded situations the events preceding this breakdown are also of considerable interest. These events are concerned with charging and charge dissipation, leading to electrical breakdown of the propellant binder. Consequently, the mechanism of Larson and Beale [5] was re–examined with particular emphasis on the portion prior to microarcs within the propellant.

Larson and Beale [5] develop a scenario in which triboelectricity is responsible for the initial charge generation, and charge separation results from relative motion (lifting a motor from a shipping container, core pulling during motor manufacture, etc.). These steps are summarized in the first line of the mechanism shown in Fig. 4. In an experiment in which propellant is placed between electrodes, the mechanism begins at line two with application of an electric field and is similar to that shown in Fig. 2. Field

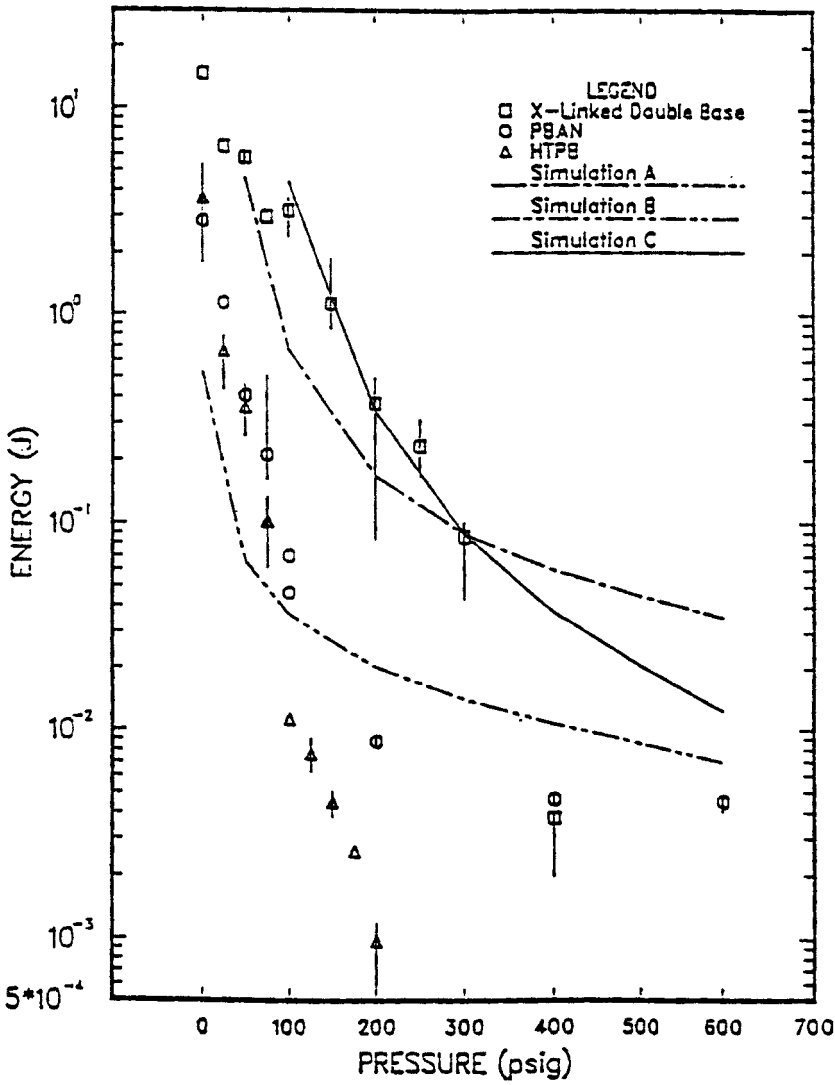

FIGURE 3

Measured and computed electrostatic discharge ignition energy versus ambient nitrogen pressure for three solid rocket propellants [9].

1. Triboelectric charging and charge separation occurs
2. High voltage and electric field result
3. Field amplifies within propellant due to closely spaced Al particles
4. Local field exceeds breakdown strength of oxide layers on Al and binder
5. Binder breakdown occurs locally in microarc(s)
6. Heat is produced
7. Binder material vaporizes and/or pyrolyzes
8. AP is available near hot binder
9. Binder decomposition products react with AP
10. Propellant stress relieves as local pressure builds due to formation of gaseous products
    - High confinement suppresses venting via cracks
11. Heat release rate due to reaction exceeds heat loss rate
    - Breakdown shock, venting through cracks, and conduction are loss mechanisms
12. Sustained combustion occurs locally
    - High confinement favors coalescence of hot spots
    - High confinement suppresses venting via cracks

FIGURE 4

Mechanism for ESD ignition in practical situations.

amplification within the propellant occurs because of the small distance between neighboring Aℓ particles. Breakdown results between two particles when the local field strength becomes sufficient to cause a microarc through the intervening metal oxide layers and binder. Lines three and four in Fig. 4 summarize these steps. Line five emphasizes the microarc concept, and the resulting arcs or microarcs produce heat, although not in the sense of thermal equilibrium.

At this point (line seven), following Isom and Speed [4], binder material vaporizes, most likely accompanied by pyrolysis. The resulting decomposition products react with AP in the vicinity of the discharge path (since Fig. 4 shows events leading to ignition, AP must be in the vicinity of the binder, line eight). Pressure buildup and maintenance to accelerate reaction involve dynamic mechanical properties of the propellant during this process, and large propellant confinements suppress fracture and venting of the reaction products.

The next requirement for ignition, the sole result of the steps shown in Fig. 4, is that the heat release rate as a result of reaction is greater than the rate of heat loss, so that hot spot temperature rises with time. The substep repeats the loss mechanisms discussed by Baker et al. [2] in terms of the initial rate and duration of the charge dissipation process. Finally, local combustion follows ignition, but the extent of propellant consumption depends on confinement. If large, then ignition sites (i.e., where AP is sufficiently close to microarc locations to allow self–sustained reaction) have

adequate time to coalesce, because high confinement also suppresses fracture.

The role of conduction heat transfer as a hot spot quench mechanism (see Step 11 in Fig. 4) is clarified in the following. As noted previously, Baker et al. [2] suggested that due to the small thermal diffusivities of typical solid composite rocket propellants, relatively long times, on the order of hundreds of μs, would occur after the initial stimulus before substantial heat could be conducted away from the hot spot site. We have examined that hypothesis for the experiments with embedded electrodes performed by Hodges et al. [9], results of which are shown in Fig. 3.

The simulation results, also shown in Fig. 3, were obtained from a transient, one–dimensional analysis of a pocket created by the spark discharge internal to the propellant [14, 9] with primary heat loss mechanism conduction into the solid propellant. Order of magnitude analysis using parameters from the simulation [14] allows examining the hypothesis of Baker et al. [2] that this method of quenching is important only for longer spark durations for the conditions of the experiments and propellants of Fig. 3. First, we estimate the heat released if a sphere of diameter equal to the spark gap is burned:

$$Q_{rxn} = \Delta h_{rxn} \rho_p \frac{4}{3} \pi [L/2]^3 \qquad (1)$$

where Δh_{rxn} is the specific enthalpy of reaction, ρ_p is the density of the solid, and L is the spark gap width. Taking values as in Table 1, Q_{rxn} is 6.53 J, larger than most of the spark ignition energies reported in Fig. 3.

TABLE 1.

Parameters Used in the Analysis of Conduction Heat Transfer From a Hot Spot, Based on Raun [14].

Parameter	Value
Δh_{rxn}	6.816 MJ/kg
ρ_p	1.83×10^3 kg/m^3
L	10^{-3} m
α_p	1.594×10^{-7} m^2/s
c_{pp}	1.2×10^3 J/kg K
ΔT	250 K
t	10^{-4} or 0.15 s

If we assume that the characteristic heat transfer thickness of a shell of solid propellant adjacent to the spherical pocket is r, evaluated using the propellant thermal diffusivity, α_p, and the spark duration, t:

$$r = \sqrt{\alpha_p t} \tag{2}$$

then the conduction to heat the shell an increment in temperature ΔT is:

$$Q_{cond} = c_{pp} \Delta T \, \rho_p \, \frac{4}{3}\pi \left[((L/2) + r)^3 - (L/2)^3\right] \tag{3}$$

where c_{pp} is the specific heat of the solid propellant. The fraction of chemical heat release used to heat the shell of propellant is thus:

$$Q_{cond}/Q_{rxn} = c_{pp}\Delta T \left[\{1 + (2\sqrt{\alpha_p t}/L)\}^3 - 1\right]/\Delta h_{rxn} \tag{4}$$

We take as typical spark durations either 100 μs or 150 ms and evaluate Eq. (4) using typical propellant properties as listed in Table 1. The temperature increase is based on an initial temperature of 300 K and an assumed surface temperature of 550 K. For the shorter duration, r, the conduction heat transfer zone thickness in the solid, is 4 μm and

$$Q_{cond}/Q_{rxn} = 0.0011 \qquad (5)$$

while for 150 ms, r = 155 μm and

$$Q_{cond}/Q_{rxn} = 0.0547 \qquad (6)$$

Thus if a sphere of diameter L burns as a result of the electrostatic discharge, then as spark duration decreases, very little of the chemical energy released is transferred away by conduction in a time equal to the duration (0.11% for 100 μs duration, as given by Eq. (5)).

However, as was noted above, Eq. (1) gives a chemical heat release substantially larger than most of the delivered spark ignition energies shown in Fig. 3. Thus, one can also use the ignition energies in the figure to normalize the conduction heat losses. If duration is varied in order to change the spark energy deposited, smaller energies require shorter durations. Taking 10^{-3} J as typical of the spark ignition energy at high ambient pressures in Fig. 3

$$Q_{cond}/E_{spark} = 7.18 \quad (7)$$

Equation (7) indicates that the conduction heat transfer is greater than the delivered energy when both are evaluated in terms of the spark duration of 100 μs. The conclusion is that conduction heat transfer cannot be ignored, even at spark durations of 100 μs or less for spherical spark kernels of diameter equal to the spark gap, and thus the loss mechanisms discussed by Baker et al. [2] have been revised (see line 11 in Fig. 4).

PROPELLANT PROPERTY EFFECTS

Thermochemical, thermophysical, chemical kinetic, mechanical and electrical propellant properties all affect the probability of and energy requirements for ignition of a solid rocket propellant by ESD. The first two categories impact the response of the binder to the microarc(s), as it starts to vaporize and pyrolyze in line seven of Fig. 4. Energies required and heat dissipation abilities are important here and in the last two lines, as was shown in the previous section. Kinetic effects also determine the rate of reaction of binder decomposition products with oxidizer (line nine) and the magnitudes of the heat release and flame spreading rates (final two lines). Thermal and kinetic parameters of importance are discussed in detail below.

Electrical properties are predominant in the first six lines which involve the electrical failure of the propellant and/or binder (breakdown voltage), the ability of the former to store charge (dielectric constant), and the

resistance to flow of current, both before and after the discharge (surface and volume resistivities). Field amplification effects and the probability of AP positioned near the location(s) of the breakdown also depend on propellant thermochemistry (through its composition and stoichiometry) – a combined thermochemical/electrical property is the percolation coefficient (see for example [15]) that is computed from binder resistivity, metal and oxidizer particle sizes and concentrations, etc.

Finally, mechanical properties play their role as pressure builds up in the hot spot(s) due to the onset of chemical reaction. In line ten of Fig. 4, depending on the pressure and its rise rate and competition between yield and fracture limits of the material, cracks reaching the propellant surface, capable of quenching the reaction, may form. Such issues have been discussed by Baker and Mellor [10], who present an analysis concerned with mechanical response to a chemically reacting hot spot.

Present experiments on and theoretical models for electrostatic discharge ignition of solid propellants are in their formulative stages. Therefore, the spark ignition literature for premixed gaseous and liquid fuel spray–air mixtures was examined for potential applicability to ignition by electrostatic discharge for solid propellants. The case of premixed gases is analogous to homogeneous propellants, while a dispersion of fuel drops in air resembles a composite propellant. The review is largely restricted to quiescent gas or fuel spray/air mixtures, that is, cases for which no velocity relative to the spark electrodes is present. It is felt that this situation is more relevant to the solid propellant case than that with a bulk gas motion. The review is also

concentrated on the last ten years, since a similar survey (primarily on experimental work) was conducted in 1987 [1].

Engineering models for spark ignition are concerned with predicting the minimum ignition energy ($E_{ig,min}$) at the optimum spark gap between the electrodes as a function of fuel type, temperature, equivalence ratio, etc. They are based on the (stationary) energy balance used in line 11 of Fig. 4 to define ignition. Such models utilizing characteristic times have been applied successfully in the past to gaseous fuel/air mixtures and fuel sprays in air [16; 17]. More fundamental computer–based solutions of the time–dependent conservation laws are now appearing in the literature for gaseous mixtures and solid propellants. Both types of models have relevance to the problem of interest because ideally they will identify thermochemical, thermophysical, and kinetic properties of a propellant which make ignition and combustion more likely given an electrostatic discharge.

In the remainder of this section, spark ignition of gaseous mixtures of fuel with air will be reviewed first. Next, spark ignition of liquid fuel spray–air mixtures will be examined. Finally, ESD ignition results for solid propellants will be discussed.

SPARK IGNITION IN HOMOGENEOUS GAS MIXTURES

Experimental Results

Spark discharges in gases are composed of three different discharge modes: breakdown, arc, and glow. The values given here for voltage,

current, and time are for gaseous mixtures and should not be applied to the solid propellant case. They are presented only to show that the three discharge mechanisms operate in different energy regions.

The breakdown phase precedes the other types and is characterized by very high peak voltages (~ 10 kV) and currents (~ 200A) along with a very short duration (<10 ns). After breakdown occurs ionizing streams propagate from one electrode to the other. The impedance of the gap between the electrodes is reduced greatly when a streamer reaches the opposite electrode and consequently the energy sent through the gap is transferred almost without loss. This causes a sudden pressure and temperature increase in the channel of ~ 20 MPa and ~ 60000 K which results in the formation of a blast wave [11] that will be discussed below.

The arc discharge phase is characterized by a very low voltage (~ 100 V) with the current limited only by the impedance of the external circuit. Its duration is ~ 0.1 ms. The glow discharge phase has currents less than 200 mA and voltages in the range of 300–500 V. Ignition energy is dependent on which type of discharge occurs [11].

Breakdown can be followed by either an arc or glow discharge, as discussed above. Ziegler et al. [18] performed measurements in lean CH_4/air mixtures at room temperature and 2 bar with various electrode materials. For spark gap L, they established that breakdown voltage V_b varied as the square root of L, not directly with L as given by Paschen's law. The energy delivered to the medium in the gap during the breakdown phase, E_b, was approximately equal to $0.5CV_b^2$, where C is the stray capacitance associated

with their electrodes (2.2 pf). Thus E_b goes directly with L. Champion et al. [19] also discuss methods to estimate the energy delivered during the breakdown phase.

This rapid release of breakdown energy generates a blast wave, originally cylindrical, traveling supersonically away from the discharge column [20]. Laser schlieren studies of the early flame kernel attribute the observed surface waviness to turbulence produced by the blast wave [21]. Maly and Vogel [11] postulated that the gas motion following the blast wave away from the kernel will induce a flow along and parallel to the electrodes, so that the gas just behind the blast wave is hot and, for sufficiently short breakdown arcs, surrounds a cool core. Thus a hot temperature shell is expected during the breakdown phase [22]. Subsequent interferometric measurements interpreted via Abel inversions by Kono et al. [23], and Rayleigh scattering results reported by Borghese et al. [24], verified the shell structure, anticipated in these experiments because the spark durations used were 0.3 μs and 0.05 μs, respectively. In the section involving detailed computation models (below) we will return to the fluid flow pattern produced in the early stages of the discharge; analyses involving conservation of momentum are becoming available, and their results show the features of blast waves and induced flows discussed above.

Borghese et al. [24] utilized ultrashort (~ 50 ns) spark durations in pure N_2 and computed from Rayleigh scattering measurements radial profiles of N and N_2 mole fractions perpendicular to the spark axis. At a time of 7 μs after the spark, nearly complete dissociation was observed on this axis,

falling to zero dissociation 2 mm from the axis for gap width L also equal to 2 mm. These workers argue that the blast wave has weakened sufficiently by this time that the initial pressure on the axis has returned to its value before the spark was fired, and using this value, the ideal gas law, and their measured total density compute a translational temperature of only 2500 K, thus demonstrating the highly nonequilibrium nature of the spark channel at this time.

After breakdown, if the external power supply and circuit permit, then either an arc or glow discharge is obtained. It is interesting to note in the context of metallized propellants that Ziegler et al. [18] did not observe the glow mode with Aℓ electrodes, which they attributed to the presence of the $A\ell_2O_3$ film on the metal surfaces. Higher currents and lower voltage drops are associated with arcs, as noted above. Kono et al. [25] investigated both DC and AC discharges and found optimal spark durations for minimum ignition energies were from 50 to 300 μs and about the same for both types of input power. Their DC cases were breakdown plus glow, except at high power levels, where they obtained breakdown plus arc discharges. They found, however, that spark energy provided a superior correlation of their ignition data than spark power. Fluid flow effects are dissipated during these longer duration sparks, so that the kernel is expected to exhibit a more uniform temperature [22].

Energy will be lost from the spark kernel to its surroundings by conduction, thermal radiation, laminar or turbulent forced convection, and shock loss. During the ignition of the spark kernel up to 50% of the energy

can be lost due to the blast wave following the breakdown discharge [26]. For ESD, only conduction, shock loss, and forced convection (if cracks develop in the solid propellant) are applicable, as will be discussed in a later section.

In early experimental studies, the actual energy delivered to the medium within the spark gap was taken as the energy stored in the external capacitor bank ($0.5CV^2$), as in the results of Kono et al. [25], but in more recent work the voltage across the electrodes and current flowing through the gap as functions of time are measured. The integral over time is taken as the spark energy. However, this latter approach ignores the electrode fall regions [22, 18, 27, 28]. Ziegler et al. [18] note the cathode fall is on the order of hundreds of volts because electrons are emitted from the cathode primarily by ionic bombardment in the glow discharge. For the arc mode, this magnitude decreases to tens of volts since thermionic and field emission are the mechanisms, and the fall region extends about 1 μm from the electrode. In either case, the anode fall is approximately the ionization potential of the intervening gas. The remainder of the discharge channel is referred to as the positive column.

These investigators thus write a sum of voltage drops

$$V_{tot} = V_{fall}(\Sigma \text{ for cathode and anode}) + (\Delta V/\Delta L)L \qquad (8)$$

where V_{tot} is the measured voltage frequently integrated over time to obtain

the delivered spark energy, as noted above, and the second term in Eq. (8) accounts for the positive column. Values of this voltage gradient were correlated for various electrode materials with the expression

$$\Delta V/\Delta L = BI^{-n} \tag{9}$$

Here n and B are constants the magnitudes of which depend on electrode material. Since the ignition energy E_{ig} is composed of both breakdown and glow or arc contributions $E_{g,a}$:

$$E_{ig} = E_b + E_{g,a} = 0.5CV_b^2 + \int_0^{t_{ig}} V_{g,a} I_{g,a} dt \tag{10}$$

where the last term is the power delivered during the glow or arc mode integrated from time zero to the ignition time.

For square wave voltage and current time histories and substituting Eq. (8) and (9)

$$E_{g,a} = V_{g,a} I_{g,a} t_{ig} = LBI_{g,a}^{1-n} t_{ig} + V_{fall,g,a} I_{g,a} t_{ig} \tag{11}$$

Also, taking $E_b = AL$, as discussed previously, Eq. (10) becomes

$$E_{ig} = AL + LBI_{g,a}^{1-n} t_{ig} + V_{fall,g,a} I_{g,a} t_{ig} \tag{12}$$

$$= E_b + E_{col,g,a} + E_{fall,g,a} \tag{13}$$

Eq. (13) shows that the energy delivered across the spark gap includes terms due to the breakdown phase, the positive column, and the anode and cathode fall regions. Ziegler et al. [18] conclude that the fall energy is lost to the electrodes because the fall region thickness is only on the order of μm and thus does not contribute to heating of the intervening medium.

In various experimental studies, a number of workers have noted that the probability of ignition is a function of the delivered spark energy [25, 18, 27]. Data of this type lead to graphs of percent of ignitions versus stimulus level (spark energy in these cases) on probability paper, or probit curves, familiar to those who perform safety studies, including systems with solid propellants. For the tests cited, minimum spark ignition energy [1] is taken as the 50% go/no go energy, that is $E_{ig,min} = E_{50}$ (Esseghir and Polymeropoulos [29] utilize an alternative approach, however), and correlations of this parameter are the results of engineering models for spark ignition in gaseous media.

Engineering Models

The origin of the engineering models is the thermal ignition theory developed by the Russians Semenov, Zeldovich, and Frank–Kamenetskii before the Second World War. The text by the latter [30], in English, is an excellent summary of this work. The approach was to solve numerically (by hand) the time–dependent conservation of energy equation for cases where the input energy and heat losses are such that the control volume can self–heat, but not ignite. The energy source is external to the vessel, that is,

its walls are hot. To facilitate these hand calculations, two essentially equivalent approaches were used: the stationary theory, in which the time dependence is ignored because only those solutions involving slow, self–heating up to and including the ignition temperature (an unstable equilibrium) are sought; and the nonstationary theory, where the control volume is assumed at uniform temperature except for boundary layers at its walls (that is, fast conduction heat transfer within the medium). Analyses reported in the mid–1960s [31] added conservation of one chemical species (a critical free radical) to the problem so that chain and thermal ignition could be treated simultaneously (the unified theory).

The stationary theory for thermal ignition defines temperatures at which solutions of the time–independent energy equation can be obtained:

$$\dot{q}_{chem} = \dot{q}_{loss} \tag{14}$$

where the first term is the chemical heat release rate and the second is a conduction heat transfer rate expression which has as boundary the heated vessel wall. One solution is a stable equilibrium at a low temperature, representing slow, steady oxidation at say room temperature. At a higher temperature, another solution, the ignition temperature, is found which is unstable, that is, if the temperature is perturbed, it will continue to change spontaneously in the same direction. After nondimensionalization of Eq. (14), one dimensionless parameter is found whose value for a particular initial wall temperature, vessel dimensions, fuel/oxidizer mixture, etc.

separates the regions of stable (no ignition) and unstable (ignition) solutions. This parameter is a Damköhler number, Da, defined as the ratio of two characteristic times:

$$\mathrm{Da} = \tau_{sl} / \tau_{hc} \tag{15}$$

Here τ_{sl} is the conduction heat transfer time for the stagnant medium heated by the confining walls and τ_{hc} is the ignition delay time for the mixture. Critical values of Da, all of order unity at the ignition limit, were obtained by solution of Eq. (14) for spherical, cylindrical, and plane–walled vessels. For values of Da in excess of the critical, ignition will occur. In this case conduction heat transfer cannot dissipate the heat released by chemical reaction.

Peters [17] formulated an engineering model for quiescent homogeneous mixtures using Eq. (15):

$$\tau_{sl} \geq \mathrm{Da}_{crit}\, \tau_{hc} \tag{16}$$

The equation above indicates that ignition will always occur if the left–hand side exceeds the right–hand side. Thus the limit for ignition is when the two sides are just equal. The slope of the equation is the critical Damköhler number.

The characteristic times τ_{sl} and τ_{hc} are estimated based on quantities known if given the macroscopic parameters of the system (pressure,

composition, temperature, etc.). The fluid mechanic or heat transfer time is defined [17]

$$\tau_{sl} = \pi d_q^2/\alpha_a \tag{17}$$

assuming that the spark kernel is spherical where α_a is the thermal diffusivity of air, and d_q is the quenching distance, defined by the equation

$$d_q = \left[\frac{E_{ig,min}}{\pi \rho_a c_{pa} \Delta T_\phi / 6}\right]^{1/3} \tag{18}$$

where $E_{ig,min}$ is the minimum ignition energy, ρ_a is the density of air, c_{pa} is the specific heat of air, and ΔT_ϕ is the adiabatic flame temperature rise at the equivalence ratio ϕ. Peters [17] evaluated α_a, ρ_a, and c_{pa} for air at 1300 K strictly for convenience; properly they represent properties of the gas in the spark kernel.

The ignition delay time is defined as

$$\tau_{hc}\,(\text{ms}) = \frac{10^{-5}\exp(E/RT_\phi)}{\phi \rho_a} \tag{19}$$

where E is the activation energy, taken as 26,100 cal/gmol for hydrocarbons with molecular weight larger than that of methane [32], R is the universal gas constant, T_ϕ is the adiabatic flame temperature, and ρ_a is expressed in units of kg/m^3. The pre–exponential factor was chosen to give the kinetic

time the order of magnitude of ms in flowing mixtures; the value used in Eq. (19) leads to a value of slope in Eq. (16) on the order of 10^3, however. Peters [17] utilized lean C_3H_8/air and C_5H_{12}/air quiescent mixture spark ignition data to develop model constants in Eq. (16), as shown in Fig. 5.

Detailed Computational Models

The traditional approach for analysis of combustion situations not involving detonation is to assume pressure remains constant and omit the conservation of momentum equation from the problem solution. As discussed above with respect to the thermal and unified theories, a typical starting point is solution of the conservation of energy and mass equations with the next sophistication involving a conservation of critical species equation. The summary below shows that a similar hierarchy has been employed in analyses of spark ignition in quiescent gas mixtures. Section (1) is concerned with studies in which the momentum equation is ignored in the time–dependent solution, while approaches including this equation in order to predict the pressure and flow fields are reviewed in Section (2).

(1) Excluding Conservation of Momentum – These literature analyses are analogous to the non–stationary thermal and unified theories summarized above, except that hand solutions are no longer necessary to perform the numerical integrations of appropriate time–dependent equations and the high temperature stable solution (steady combustion) is found as well.

Adelman [33] argued that since the initial kernel growth is similar for

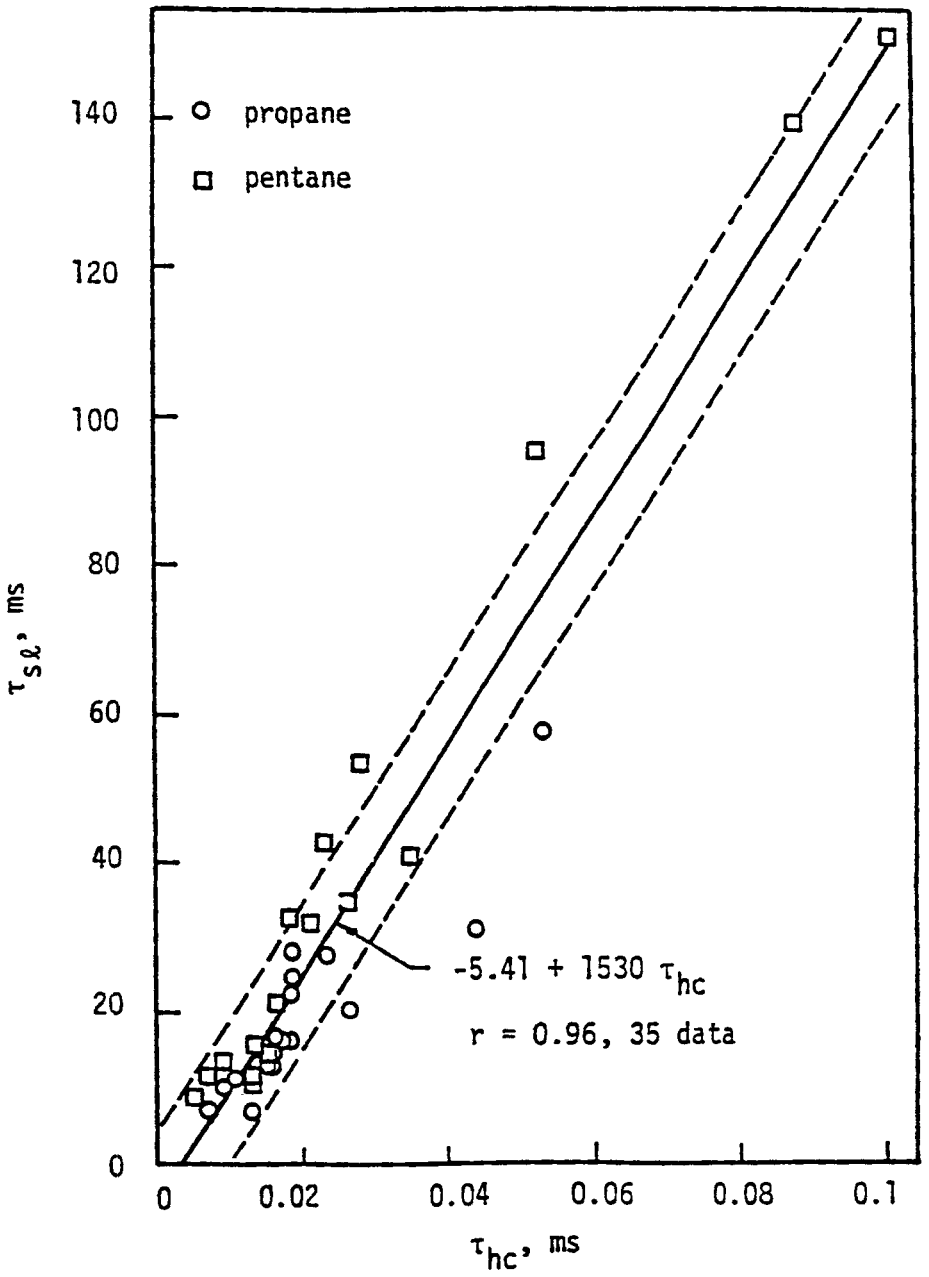

FIGURE 5

Characteristic time model ignition correlation of data from Fenn [32] obtained by Peters [17].

sparks in air or in fuel/air mixture, chemical heat release can be ignored. He solved the time–dependent energy equation with a prescription for input spark energy as a function of time. Conduction, convection, and radiation heat losses were ignored, and his solutions indicated good agreement with experimental data for blast wave and kernel radii versus time from zero to 1 ms reported by Litchfield in 1961.

Inclusion of the species conservation equation for limiting reactant (fuel in a lean system) and kinetics overall first order with respect to this species was reported by Champion et al. [19]. A stability analysis was also performed upon the solutions of a stationary approach. Comparison with experiments of Kono et al. [25], as well as their own, was limited to verification of the computed trend of an optimum spark duration at which ignition energy is a minimum.

Dimensional analysis including the momentum equation was used by Lim et al. [34] to examine the blast wave and establish initial conditions for the time–dependent mass and energy equations. Global chemistry was included through use of a laminar flame speed, which in general is a function of fuel, fuel/air ratio, and initial mixture temperature and pressure. Electrode heat losses were modeled by subtracting out the cathode and anode falls from the total voltage drop (see Eq. (8)). The theory exhibited good agreement with kernel growth time histories to 1.6 ms measured by Lim. It was also found that the spark's contribution to the total kernel energy was from 10 to 30%, increasing with increasing spark energies in the range associated with gaseous hydrocarbon/air ignition at standard temperature

and pressure (order of mJ to tens of mJ). This is three orders of magnitude greater than that for solid propellants, obtained by combining Eq. (5) and (7).

The work of Ko et al. [35] is similar to that of Lim et al. [34] except that conservation of critical species and a first order overall chemical reaction are included. Predictions of kernel growth rate compared favorably with experiment to times as long as 20 ms, as seen in Fig. 6.

Sher and Refael [36] was the first of a series of papers that utilize a detailed, 18 step CH_4/air kinetic mechanism and solve the time–dependent energy, species, and mass equations. Time histories of each species are predicted by the model, as is the growth of the kernel. The authors indicate that no appropriate experimental data exist, so there is no comparison with measurements. Refael and Sher [37] report a similar analysis except now both an I^2R term for channel heating, using a model for the electrical conductivity of air as a function of temperature and pressure, and a radiation heat loss term are included. Results show the kernel spatial extents at times of 70 μs and less for fuel/air mixture exceed those for air due to the chemical heat release. Parametric studies with this model, reported by Sher and Keck [38], demonstrate that increased breakdown energies or spark durations will increase the rate of flame spread, but again model predictions are not validated with experimental data.

(2) Including Conservation of Momentum – In addition to the blast wave dimensional analysis of Ko et al. [35] mentioned above, other

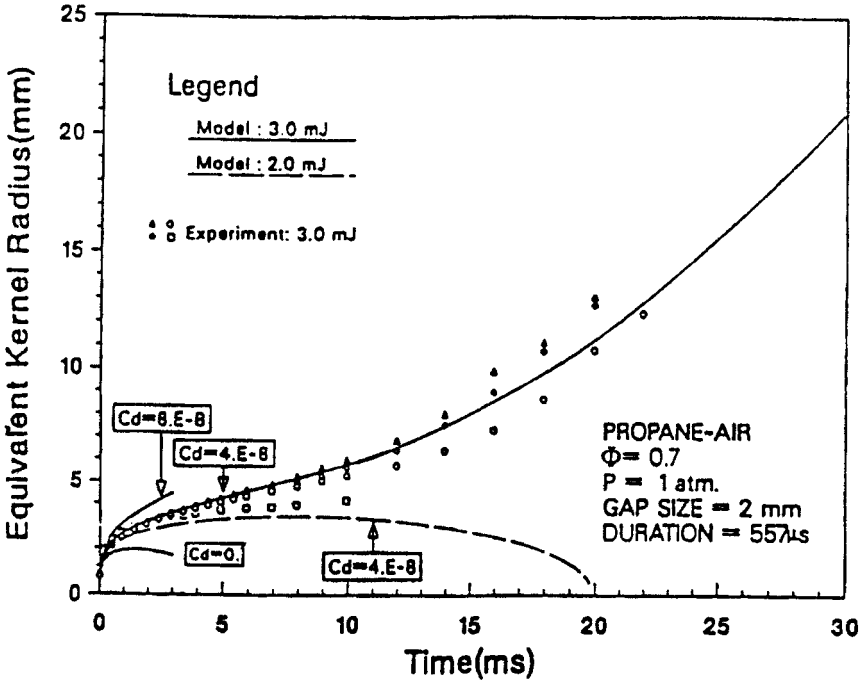

FIGURE 6

Comparison of predicted and measured kernel radii in a propane–air mixture [35].

investigators have cited literature or performed closed form studies of this phenomenon important to the initial portion of a discharge. Syage et al. [39] used lasers to induce sparks for ignition of gaseous mixtures and noted that the Taylor blast wave model predicts the following velocity v and position r of the blast wave

$$v = \frac{2}{5}(E/\rho_0)^{1/2} r^{-3/2} \tag{20}$$

$$r = (E/\rho_0)^{1/5} t^{2/5} \tag{21}$$

where E is the energy deposited instantaneously in a gaseous medium of density ρ_0. Note that the model predicts blast wave radius grows with the 2/5 power of time, t. In contrast, Au et al. [40] predict growth with the 1/4 power of t from their analysis based on hydrodynamic puff theory. Borghese et al. [24] report correlation of experimental, laser schlieren measurements of equatorial (maximum) blast wave radius for short duration sparks in N_2 at atmospheric pressure and temperature with

$$r^2 = r_0^2 + k_1 t + c^2 t^2 \tag{22}$$

where $r_0 = 0.76$ mm, $k_1 = 1.87$ m^2/s, and $c = 350$ m/s, the sound speed in N_2 at the undisturbed conditions. These workers note that the second term in Eq. (22) is consistent with the strong shock theory of Landau and Lifshitz for a cylindrical geometry

$$r^2 = b\,(E/\rho_0 L)^{1/2} t \qquad (23)$$

if b is about 0.8 for their results.

Because puffs not only conserve momentum, but also by definition entrain fluid in proportion to their surface area, Au et al. thus are able to model the relevant fluid flow into the kernel (see also [35] for a discussion of modeling this entrainment via Cd in Fig. 6). Au et al. show reasonable agreement of their model and experiments for kernel positions at times as long as 4 ms and as a result suggest that the flow subsequent to blast wave expansion may be dominated by the puff instead of by heat and mass transfer from burned to unburned gases, as in the analyses discussed in Section (1).

Undoubtedly the most complete numerical computations examined are those of Kono et al. [23] and Ishii et al. [41] who applied the RICE code from Los Alamos and solved the time–dependent conservation equations for mass, momentum, and energy in cylindrical coordinates for short duration sparks (and thus in their early work argued that chemistry was negligible but included a one–step global rate in the more recent study). An example of the computed flow pattern at 100 μs is shown in Fig. 7, and the evolution of the hot kernel with toroidal shape resulting from this flow is shown in Fig. 8. Note that the predicted flow is entirely consistent with that envisioned by Maly and Vogel discussed previously. Unfortunately, no computed results for the blast wave per se are presented by Kono et al. [23].

The model developed by Bradley and Lung [42] focused in part on this

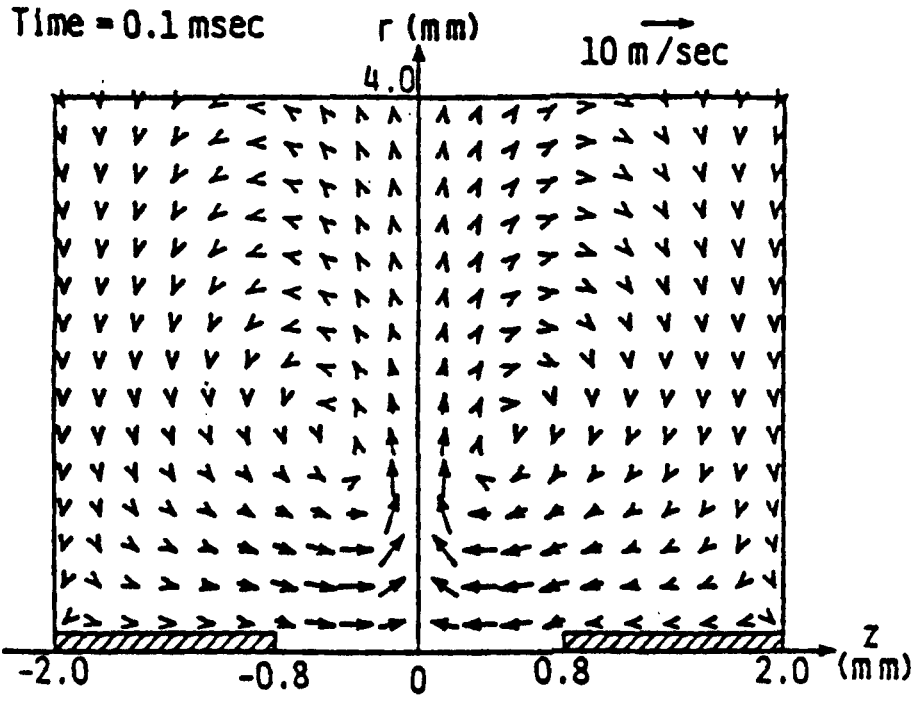

FIGURE 7

Computed gas flow pattern and velocity magnitudes for 1.6 mm spark gap between 0.2 mm diameter cylindrical electrodes shown on x–axis 100 μs after an instantaneous spark of 2.08 mJ [23].

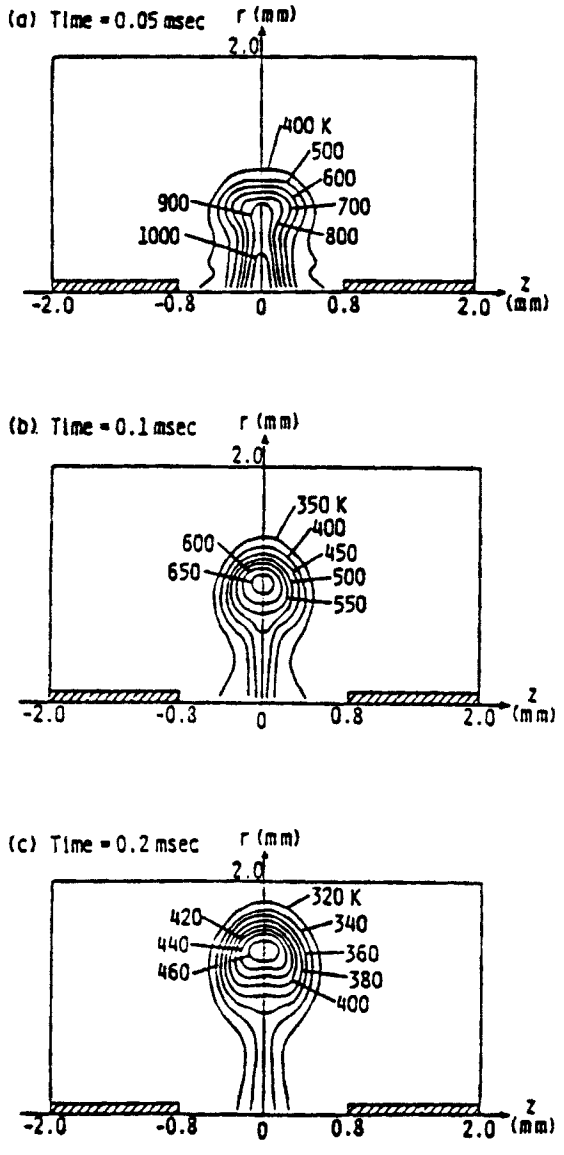

FIGURE 8

Computed temperature spatial distributions at (a) 50 μs, (b) 100 μs, and (c) 200 μs computed for spark of Fig. 7 [23].

early portion of the process. Time–dependent mass, momentum, and energy conservation equations were solved numerically for an axisymmetric, long right cylinder with initial conditions selected from the literature to correspond to the post–breakdown conditions in the spark channel. Chemistry was also ignored in this model. Figure 9 shows typical results for the blast wave, at times after breakdown of 10, 15, and 20 μs. The dissipation of this wave is clearly indicated. Based on Weinberg's work, a computed temperature of 450 K was taken to characterize maximum deflection in schlieren measurements in reacting systems, so that the flame kernel radius versus time could also be deduced from the calculations. Figure 10 compares both blast wave and flame kernel trajectories from the theory with measurements (dashed lines) reported by Ziegler et al. [18]. In the analysis, various spark energies and durations subsequent to breakdown were selected. Although the results show little effect on the blast wave, which is dominated by the initial conditions selected, there is a large influence on the kernel growth. Bradley and Lung [42] attributed the difference in spark energies to match the kernel spread rate (1 mJ in the experiments versus 3 to 9 mJ in the computed results) to their model's omitting any effects of chemical heat release: the measurements were performed in lean CH_4/air mixtures [18].

As was noted, global finite–rate chemistry was added to the simulations of Kono et al. [23] by Ishii et al. [41]. The latter investigators show a spherical blast wave at 4 μs for spark duration of 2 μs, qualitatively confirming the results of Bradley and Lung [42] shown in Fig. 9. In addition,

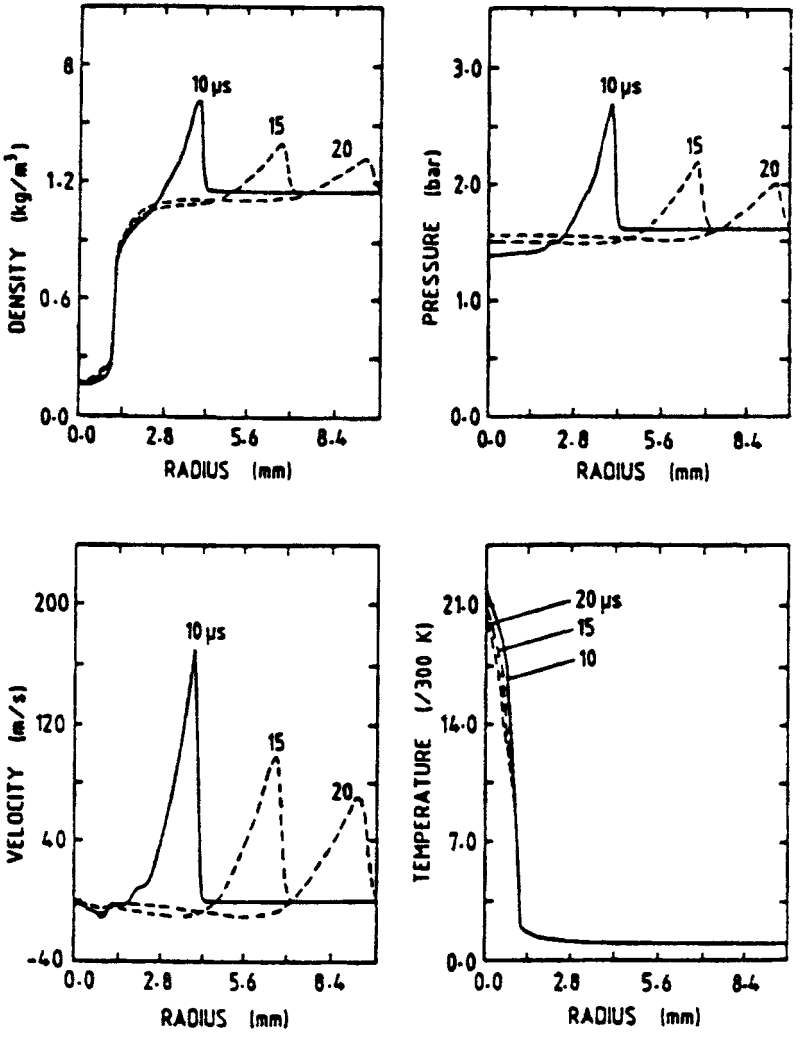

FIGURE 9

Computed radial profiles at three times after breakdown for gas density, pressure, radial velocity, and temperature. 2 mm spark gap, spark duration of 770 μs, and spark energy 10.1 mJ (excluding breakdown; [42]).

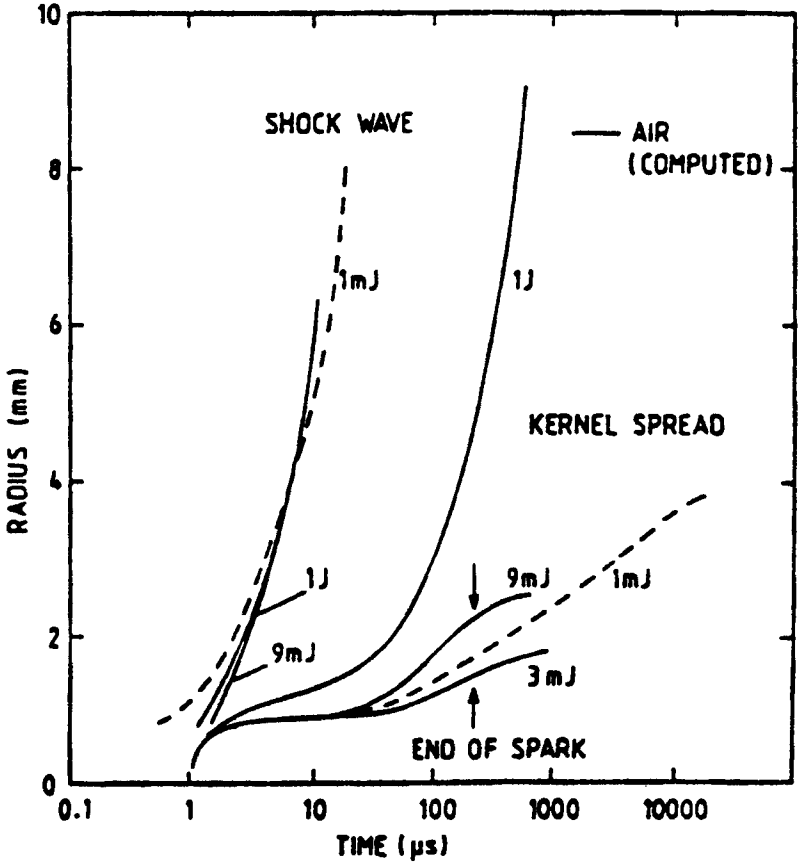

FIGURE 10

Experimental ([18], results of which are indicated by the dashed lines) and computed blast wave and flame kernel trajectories, from Bradley and Lung [42]. See text for details.

with inclusion of both chemical heat release rate and heat loss to the electrodes, Ishii et al. [41] were able to predict the existence of the minimum spark ignition energy, for variations in spark duration.

Properties which Favor Ignition

In addition to developing insight into the spark ignition process and establishing the state of the art of experiments and modeling, another goal of the present study was to determine which properties of the combustible medium influence ignitability and resulting combustion. For quiescent gaseous mixtures, very few parametric studies involving these properties with the detailed computational models have been identified, and thus we will use the engineering model for our present purposes. Because this model is thermal in nature, it will identify thermal and chemical properties which favor combustion.

Figure 5 shows the following correlation equation, obtained for two hydrocarbon fuels in air:

$$\tau_{sl} = 1530\tau_{hc} - 5.41 \qquad (24)$$

where τ_{sl} is defined in Eq. (17) and τ_{hc} is defined in Eq. (19).

Equation (24) is the correlation of the ignition limit. If conditions are such that the left hand side equals or exceeds the right hand side, then ignition will occur and combustion will follow. Thus, either increases of the left hand side or decreases of the right hand side will facilitate ignition.

Equivalently, large values of τ_{sl} and small values of τ_{hc} lead to more probable ignition. From Eq. (17) the former occurs with small mixture thermal diffusivities (so that conduction away from the kernel is small) and large quenching distances (or, from Eq. (18), spark energy inputs greater than the minimum raise a larger volume of the gas to its flame temperature). Similarly, Eq. (19) indicates that high gas densities (or pressures), lean equivalence ratios near stoichiometric (where $\phi = 1$), low activation energies, and high flame temperatures (also near stoichiometric) favor sustained combustion given a certain level of spark input energy.

SPARK IGNITION IN FUEL SPRAY/AIR MIXTURES

In the previous section, premixed combustible gaseous mixtures stationary with respect to the inserted electrodes were considered. We believe this case is analogous to that of embedded electrodes in a homogeneous double base propellant, where reactants are mixed on a scale much smaller than the electrode diameter or spark gap width. The situation reviewed in the present section, fuel droplets and/or sprays dispersed in air, is similarly analogous to composite propellants, where solids (AP and Aℓ) are dispersed in binder.

Experimental Results

Ballal and Lefebvre [43] spark ignited quiescent mists of various liquid hydrocarbons in air. The fuels included were iso–octane, Diesel oil, and a

heavy fuel oil, lean sprays of which were suspended in stagnant air at pressures from 0.2 to 1.0 bar. As is typical practice in describing fuel sprays, the characteristic diameter reported for the spray is the Sauter mean diameter, also known as d_{32}, or the volume to surface area diameter. Experimental results indicated that good atomization promoted ignition (which for a given injector translates primarily to low fuel viscosity and resulting small Sauter mean diameter), and that fuels of high volatility ignited more easily.

Danis et al. [44] performed a more fundamental study with monodisperse sprays of normal C_5H_{12} or CH_3OH in which the droplet size, velocity, and equivalence ratio were measured in the spark gap. The percent fuel vaporized before its arrival at the gap was also deduced. Results on the effects of fuel and spray properties were found similar to those reported by Ballal and Lefebvre. Minimum spark ignition energy was defined as E_{50} on the probit curve.

Single droplets under microgravity conditions were the focus of Shaw et al. [20], and these investigators found that the spark frequently delivered sufficient impulse to ~ 1000 μm droplets that they left the gap without igniting. Their work organizes and quantifies both fluid mechanics and electromagnetic effects responsible for droplet motion in an electric field across a medium which is breaking down.

Engineering Models

Focusing again on the characteristic time approach, Peters and Mellor

[16] correlated the results of Ballal and Lefebvre [43] by replacing the chemical ignition delay time τ_{hc} in Eq. (16) with the evaporation delay time for a droplet of the Sauter mean diameter, τ_{eb}. For droplets with zero velocity relative to the ambient air,

$$\tau_{eb} = d_{32}^2/\beta \tag{25}$$

where β is called the evaporation coefficient and is a function of the liquid's specific gravity and volatility:

$$\beta = (8k_a/\rho_f c_{pa}) \ln (1 + B) \tag{26}$$

Here k_a is the air thermal conductivity, subscript f refers to the liquid fuel, and B is called the transfer number for evaporation, the ratio of the enthalpy available in the gas phase to evaporate unit mass fuel to that required to heat the liquid from its initial (T_0) to boiling temperature (T_A) and convert it to vapor at the boiling point:

$$B = c_{pa}(T_C - T_A)/[c_{pf}(T_A - T_0) + \Delta H_{vap}] \tag{27}$$

In Eq. (27) T_C is the ambient air temperature and ΔH_{vap} is the latent heat of vaporization of the liquid. Note thus that large values of B indicate volatile fuels, which in turn through Eq. (26) and (25) have high evaporation coefficients and small droplet lifetimes.

These investigators ignored chemical kinetics, that is, following Lefebvre et al. [45] and Ballal and Lefebvre [46], argued that evaporation of the fuel was limiting to spark ignition, and correlated Ballal and Lefebvre's [26] data with an expression analogous to Eq. (24):

$$\tau_{sl} = 14.2\tau_{eb}/\phi + 2.29 \tag{28}$$

with a correlation coefficient of 0.99. The definition of τ_{sl} given in Eq. (17) was retained.

However, comparisons of the correlation with experimental data indicated that the agreement worsened as equivalence ratio was reduced toward the lean limit. Consequently, Peters and Mellor [47] reinstated the kinetic time in spark ignition limit correlations for data obtained by Ballal and Lefebvre [46] in flowing sprays in air, and for two gas turbine combustors:

$$\tau_{sl} = m(\tau_{hc} + 0.021\tau_{eb}/\phi) + b \tag{29}$$

where the multiplicative factor on τ_{eb} was selected empirically to optimize the quality of the least squares fit. We omit the values of slope m and y–intercept b because they varied between the laboratory and engine datum sets (but were the same for both turbine engines), and the definition of τ_{sl} was modified appropriately since the correlations are for flowing mixtures. The definition of τ_{hc} given by Eq. (19) was retained, however, except that T_{ϕ} in the exponential is replaced with $T_{\phi=1}$, the adiabatic stoichiometric

flame temperature, because droplets are expected to ignite at stoichiometric where kinetics are fastest instead of at the overall equivalence ratio. Note that the physical interpretation of Eq. (29) is that, for ignition, the time associated with heat transfer of the spark energy away from the kernel must equal or exceed the sum of the physical delay time for evaporation and chemical ignition delay time.

Dietrich et al. [48] utilized the form of the model ignoring kinetics, Eq. (28), modified with a term on the right hand side accounting for the fraction of fuel prevaporized before droplets reached the spark gap (important for the n–C_5H_{12} experiments of Danis et al. [44]), to speculate on the non–deterministic results obtained by Danis et al., that is, the spark ignition probit curve. They measured experimentally the variation of equivalence ratio in the spark gap, as well as the variation in spark energy delivered to the gap. Standard deviations in ϕ were 50% of the mean value, and in spark energy were 10% of the mean. Assuming truncated Gaussian distributions and using Monte Carlo random walk simulations for each, a predicted ignition probit curve was generated for the experiments of Danis et al. [44]. Excellent agreement with the experimental data was obtained with theoretical predictions using the Monte Carlo approach, except in cases which were overall very lean (perhaps again suggesting that the chemical ignition delay must be included in the model, as in Eq. (29)). For a case where agreement was very good, parametric studies were made with the model on the standard deviation in ϕ. The results showed that altering the distribution in equivalence ratio changed the shape of the probit curve (thus

values of E_{10} and E_{90} for example), but that E_{50} was relatively independent of the width of the distribution. This observation supports the general practice of defining $E_{ig,min}$ as E_{50}.

Note that these results have an implication for composite solid propellants. In Fig. 4 for ignition, it is required that AP be available near the binder breakdown path so that chemical reactions begin after the microarc(s). For a propellant with monomodal AP, the analysis of Dietrich et al. [48] relates the shape of the propellant ignition probit curve to the probability that AP is in the vicinity of the discharge, or, in replicate tests, to the differences from sample to sample in the local AP loading near the discharge path. Other factors such as how the presence of AP affects the Aℓ interparticulate distance (that is, the percolation coefficient; see for example Covino and Hudson [15]) are involved as well, however.

Properties Which Favor Ignition

Because no detailed computational studies have been conducted for the spark ignition of a fuel spray in air, again the engineering model is used to clarify which parameters facilitate ignition in such a heterogeneous system. Eq. (29) shows that gas and vapor phase characteristic times ($\tau_{s\ell}$ and τ_{hc}) appear in the same fashion in the current model as in the homogeneous model, Eq. (24). Thus all properties discussed for gaseous fuel/air mixtures affect ignitability of the droplet/air mixture in the identical way (but see comments below regarding thermal diffusivity). The new parameter appearing in Eq. (29) is the mean droplet evaporation time (τ_{eb}, defined in

terms of the Sauter mean diameter of the spray). Following the same logic as used previously, small values of τ_{eb} will allow ignition of the spray at lower values of spark energy.

Equation (25) indicates that small fuel drop diameters favor ignition and combustion, and with Eq. (26) it is seen that low fuel density (or specific gravity) and high transfer number lead to the same result. Recalling that transfer number is a measure of volatility, Eq. (27) suggests high ambient and/or initial droplet temperature, low boiling point, and low latent heat of vaporization are positive factors. It is interesting to note that for liquid hydrocarbons, both neat and multicomponent, properties vary with molecular weight consistent with the above criteria: as molecular weight increases, viscosity increases (which generally causes worsened atomization and larger spray mean diameter), density increases, and volatility decreases. Thus, ignition requirements increase with molecular weight of the liquid fuel.

For gaseous fuels and air, small thermal diffusivity of the mixture is shown favorable, and in Eq. (26) thermal conductivity and specific heat of the ambient appear. The coefficient of the natural logarithm can be rewritten:

$$(8k_a/\rho_f c_{pa}) = (8k_a/\rho_a c_{pa})(\rho_a/\rho_f) \tag{30}$$

$$= 8\alpha_a(\rho_a/\rho_f) \tag{31}$$

Because the thermal diffusivity appears in the denominator of the drop

evaporation time (large values favor high conduction heat transfer from the ambient at T_C to the drop surface, which results in more rapid evaporation), this property incorrectly cancels out in the version of the model which ignores chemical kinetics (Eq. (28)).

SPARK IGNITION IN ENERGETIC MATERIALS

Experimental Results

Li and Wang [49] review literature concerned with pyrotechnics and explosives. Of special significance here are their experiments comparing the spark sensitivity of H_2/air (gaseous) mixtures, lead styphnate, and black powder using identical, photoengraved electrode sheets on which quiescent piles of the solid materials were prepared. The sheets were simply inserted into a vessel subsequently charged with H_2/air in the gaseous mixture experiments.

For all three reactants Li and Wang demonstrated the existence of a minimum spark ignition energy, $E_{ig,min}$, provided electrode gap width L and spark duration were optimized. Optimum widths were smaller than those usually observed for hydrocarbon fuels or sprays in air, which are typically on the order of 5 mm: Li and Wang report 0.5 mm for H_2/air, $\leq$ 0.1 mm for lead styphnate, and $\leq$ 0.2 mm for black powder. The optimal duration, reported as the RC time constant of the external circuit, was 10 ns for the lead compound and 2 ms for black powder. Mäki and Oy [50] also provide information on optimal durations for several explosives in terms of external

circuit resistance and capacitance. Li and Wang [49] suggest that variation of the external RC varies not only duration, but also the initial rate of application of spark energy to the samples (presumably in the breakdown phase). These workers conclude that sensitivity decreases in the order H_2/air, lead styphnate, black powder.

Mäki and Oy [50] used an apparatus reminiscent of the Bureau of Mines spark sensitivity test for quiescent piles of flammable solids [51] and discuss how the details of the hardware, including its R and C discussed above, will affect the outcome (see also [1]). Important properties of the energetic material include grain size, porosity, and water content, and of the environment include ambient temperature, relative humidity, and confinement. Li and Wang [49] report explicit correlations for $E_{ig,min}$ for black powder in terms of atmospheric temperature and humidity: $E_{ig,min}$ increases with either decreases in temperature or increases in relative humidity.

A small–scale ESD test for solid propellant cubes (rather than powders of explosives or pyrotechnics) with embedded electrodes was reported by Hodges et al. [9]. Needle electrodes were inserted into the propellant sample, but neither gap nor duration was optimized, so that the ignition energies reproduced in Fig. 3 are not necessarily minima [52].

Kent and Rat [7] originated the frequently used, large–scale ESD test, now generally termed the French test. It is designed to provide thresholds for any propellant reaction to an ESD stimulus (cracking, initiation, or ignition), but does not provide quantitative information on ignition energy [1].

Specialized test fixtures have been designed to provide optical access to the hot spots resulting from spark discharges within propellants. The ant farm procedure of Isom and Speed [4] was mentioned previously, and has provided important insight into ESD ignition mechanisms.

Detailed Computational Models

Hodges et al. [9], as mentioned previously, developed a thermal model for breakdown–induced ignition of solid propellant. In this model, di–electric breakdown inside the propellant releases energy which produces a kernel of hot gas, the temperature of which is calculated from the adiabatic flame temperature at constant volume at the overall propellant equivalence ratio plus a term accounting for the added ESD ignition energy. The propellant is treated as a homogeneous solid which burns above its ignition temperature in the gas phase in an ith order reaction (which introduces gas phase kinetics proportional to p^i).

The energy balance used is to be contrasted with Eq. (18). The latter states that at the minimum ignition energy, the spark energy heats a volume of diameter equal to the quenching distance to its adiabatic flame temperature. In contrast, Hodges et al. [9] will obtain higher kernel temperatures, because E_{ig} adds to the computed flame temperature and E_{ig} is presumably larger than $E_{ig,min}$, as discussed previously for their tests. The hot spot then expands as the propellant cracks locally to a lens–shaped volume (in a plane containing the electrodes). Propellant products of combustion cool as the pressure decreases.

Time–dependent, one–dimensional conservation equations are solved, using initial conditions estimated as above, for mass and energy in the solid phase, and for mass, reactant species, and energy in the gas phase within the hot spot. A limiting value of E_{ig} just sufficient to cause ignition was found for each ambient pressure by parametric variation in the initial condition computation. Results of the analysis are shown in Fig. 3 as Simulations A through C. Because the figure shows ignition limits, at some values of input spark energy the propellant is self–extinguishing, that is, the pressure and temperature decreases during the kernel expansion are sufficient to prevent the chemical heat release rate from exceeding the heat loss rate. This quenching mechanism is one of two studied by McHugh [53].

McHugh estimates initial conditions and propellant burn rate exactly as do Hodges et al. [9], with some exceptions. Coupled gas– and solid–phase solutions to the governing equations are then obtained with these initial conditions. As discussed by Baker and Mellor [10], McHugh [53] includes both void expansion by elastic deformation and local cracking, computed subsequent to the initial adiabatic expansion. By suitable choices of elastic modulus and fracture toughness he demonstrates a case in which the propellant ignites and burns, a case that exhibits quenching due to elastic deformation, and a case where propellant cracking causes the burn rate to go to zero. Although the effect of ambient pressure is to reduce the pressure differential driving the deformation or fracture, McHugh made all computations reported with ambient pressure set to zero, and thus no effort was made to explain the trends with pressure observed by Hodges et al. [9].

One important assumption of the model of Hodges et al. is that ignition delay times greatly exceed propellant mechanical relaxation times. Ignition delay times of one to several ms were measured by Ziegler et al. [18] in gaseous systems and are associated with kernel motion as shown for example in Fig. 6. For propellants, Mellor et al. [12] note millisecond–range ignition delays as well. Usually, chemical heat release during any ignition delay is minimal. In contrast, Hodges et al. and McHugh model combustion reactions and their associated heat release from the start of their calculations.

Properties which Favor Sustained Combustion

Nevertheless, both of these models, and the engineering models discussed previously, provide significant insight into propellant properties which facilitate ignition and combustion or alternatively make ignition more probable given a particular level of ESD energy provided to the propellant. Table 2 summarizes this information, in terms of thermophysical, thermochemical, kinetic, mechanical, and electrical propellant properties which influence sensitivity; variations which favor combustion are indicated in the table.

In the first category, low values of propellant thermal diffusivity, activation energy for ignition delay, ignition temperature, density, and, for composite propellants, average oxidizer particle size lead to high sensitivity, as do large oxidizer transfer number, propellant percolation coefficient (through solids loading), and high flame temperature (larger oxidizer and metal loadings).

Important mechanical properties depend on the choice of model for the

TABLE 2.

Propellant Properties which Favor Sustained Combustion.

1. Thermophysical, Thermochemical, and Kinetic
   - ↓ α_p, Small Thermal Diffusivity
   - ↓ E, Small Activation Energy for Ignition Delay
   - ↓ d_{32}, Small Sauter Mean Diameter for AP Size Distribution[a]
   - ↓ ρ_p, Low Propellant Density
   - ↑ B, Large AP Transfer Number[b]
   - ↑ $T_{\phi,V}$, High Constant Volume Adiabatic Flame Temperature
   - ↓ T_{ign}, Low Propellant Ignition Temperature
   - ↑ P_{imp}, High Percolation Coefficient

2. Mechanical
   - ↑ E_{el}, Large Young's (Elastic) Modulus[c]
   - ↑ K_{1c}, Large Fracture Toughness[c]
   - ↑ σ_y, Large Yield Stress[c]

3. Electrical
   - ↓ E_{bd}, Low Dielectric Breakdown Strength
   - ↑ P_{imp}, High Percolation Coefficient
   - ↑ ϵ, Large Dielectric Constant
   - ↓ $\rho_{v,bd}$, Large Post–breakdown Volume Resistivity

[a]Equivalently, high burn rate composite propellants are more likely to ignite.
[b]Composite propellants only; equivalent to low surface temperature and small enthalpy change for AP gasification.
[c]Or any other mechanical properties, according to constitutive model used, which limit deformation and/or cracking as a result of hot spot pressurization.

propellant (linearly elastic, linearly plastic for example), but values which suppress hot spot expansion through either propellant deformation or fracture enhance sensitivity. As indicated in Table 2, such properties are large elastic modulus, yield strength, and/or fracture toughness. Other properties are discussed by Baker and Mellor [10].

Finally, certain electrical propellant properties are important to ignitability, but have not been discussed in detail because the main premise was, given an ESD discharge, to develop the sequence of events which are more likely to lead to combustion. Those favoring ignition are low breakdown strength, high percolation coefficient, high dielectric constant, and low volume resistivity in the spark channel.

In addition to the propellant properties listed in Table 2, environmental parameters have important effects on sensitivity. Temperature, relative humidity, and confinement (ambient pressure, specimen size, or substantial casings) have been discussed previously. Note in reality the main influence of the first two parameters may be through variation of the propellant properties shown in Table 2. Further research to clarify some aspects of identification of the role of properties, true minimum ESD ignition energy requirements, and the mechanism leading to propellant combustion is one subject of the following section.

SUMMARY

Figure 4 represents an AP composite rocket propellant ESD ignition

mechanism believed consistent with present understanding, and Table 2 summarizes qualitatively how changes in propellant formulation philosophy to alter various properties will affect ESD sensitivity, based on information in the recent literature. Spark ignition in homogeneous gas mixtures, fuel spray/air mixtures, and energetic materials was reviewed to obtain insight into the basis for the ignition mechanism. Literature from the last ten years received emphasis, in terms of experimental results, engineering models, and detailed computational models. Measurements of ESD energy to ignite propellants via embedded electrodes have also been reported, although there are questions whether the experimental configuration and method lead to minimum values, generally thought properties for a given composition, stoichiometry, initial pressure, temperature, and relative humidity, at least for homogeneous gas mixtures and sprays of fuel droplets in air.

Follow–on studies that will clarify gaps in understanding include modeling of energy for propellant ignition by embedded electrodes with the engineering approach, and measurements of minimum energies for ignition by embedded electrodes in various geometries. Experiments on mechanical failure properties of propellants subjected to breakdown, confinement effects on breakdown threshold, and particle size distribution effects on mechanical and electrical stresses are also recommended. Finally, propellant mechanical response to various cavity pressurization rates can be modeled, all of which will provide further insight into the sensitivity mechanism shown in Fig. 4.

ACKNOWLEDGEMENTS

This work was performed under Subcontract Number D728136A2S with the TRW Ballistic Missiles Division, System Safety Section, San Bernardino, CA. We express our appreciation to R. N. Thibedeau, who served as technical liaison.

REFERENCES

1. A.M. Mellor, D.R. Stoops, T.P. Rudy and R.W. Hermsen, *Propellants, Explosives, Pyrotechnics* 15, 1 (1990).

2. P.J. Baker, A.M. Mellor and K.B. Isom, in Workshop on Propellant Ignition Micromechanics Proceedings, Army Research Office, 1991, p. 1.

3. D.A. Wiegand, in Workshop on Propellant Ignition Micromechanics Proceedings, Army Research Office, 1991, p. 149.

4. K.B. Isom and T.C. Speed, in Workshop on Propellant Ignition Micromechanics Proceedings, Army Research Office, 1991, p. 215.

5. R.W. Larson and P.D. Beale, in Workshop on ESD Ignition of Composite Solid Propellants Proceedings, Army Research Office, 1989, p. 1.

6. K.B. Isom, Discussion cited in A.M. Mellor, D.R. Dreitzler, R.W. Larson and D.M. Mann (1989), p. ii, Workshop on ESD Ignition of Composite Solid Propellants Proceedings, Army Research Office; in JANNAF Propulsion Systems Hazards Subcommittee Meeting Proceedings, CPIA Publ. 538, Vol. I, 1989, p. 219.

7. R. Kent and R. Rat, Proc. 20th DoD Explosives Safety Board Seminar, Norfolk, VA, 1982, p. 883.

8. R.W. Larson, P.D. Beale, M.F. Gyure, J.E. Lindsay, Jr. and J.D. Curry, "Microstructural modeling of electrical breakdown in solid fuel propellants," Interim Report, Contract DAAL03–87–C–0021, Army Research Office, 1989.

9. R.V. Hodges, L.E. McCoy and R.L. Raun, in Workshop on Propellant Ignition Micromechanics Proceedings, Army Research Office, 1991, p. 113.

10. P.J. Baker and A.M. Mellor, "Mechanical response of a solid propellant to an internal hot spot in an ESD event," Joint Meeting, Central States and Eastern Sections/The Combustion Institute, 1993.

11. R. Maly and M. Vogel, in Seventeenth Symposium (International) on Combustion, The Combustion Institute, Pittsburgh, 1978, p. 821.

12. A.M. Mellor, D.A. Wiegand and K.B. Isom, in Structure and Properties of Energetic Materials, Materials Research Society Symposium Proceedings 296, Pittsburgh, 1993, p. 293.

13. P.P. Budenstein, Army Missile Command, Personal communication, 1991.

14. R.L. Raun, Hercules Aerospace Company, Personal Communication, 1992.

15. J. Covino and F.E. Hudson, *J. Propuls. Power* 7, 894 (1991).

16. J.E. Peters and A.M. Mellor, *Combust. Flame* 38, 65 (1980).

17. J.E. Peters, Ph.D. Thesis, School of Mechanical Engineering, Purdue University, 1981.

18. G.F.W. Ziegler, E.P. Wagner and R.R. Maly, in Twentieth Symposium (International) on Combustion, The Combustion Institute, Pittsburgh, 1984, p. 1817.

19. M. Champion, B. Deshaies, G. Joulin and K. Kinoshita, *Combust. Flame* 65, 319 (1986).

20. B.D. Shaw, F.L. Dryer, F.A. Williams and N. Gat, *Combust. Flame* 74, 233 (1988).

21. Y. Ko, R.W. Anderson and V.S. Arpaci, *Combust. Flame* 83, 75 (1991).

22. R. Maly, in Eighteenth Symposium (International) on Combustion, The Combustion Institute, Pittsburgh, 1981, p. 1747.

23. M. Kono, K. Niu, T. Tsukamoto and Y. Ujiie, in Twenty–Second Symposium (International) on Combustion, The Combustion Institute, Pittsburgh, 1988, p. 1643.

24. A. Borghese, A. D'Alessio, M. Diana and C. Venitozzi, in Twenty–Second Symposium (International) on Combustion, The Combustion Institute, Pittsburgh, 1988, p. 1651.

25. M. Kono, S. Kumagai and T. Sakai, in Sixteenth Symposium (International) on Combustion, The Combustion Institute, Pittsburgh, 1976, p. 757.

26. D.R. Ballal and A.H. Lefebvre, *Combust. Flame* 24, 99 (1975).

27. G.T. Kalghatgi, *Combust. Flame* 77, 321 (1989).

28. R. Schneider, M. Willey, J. Faulkner, L. Shaeffer and D. Dreitzler, in JANNAF Propulsion Systems Hazards Subcommittee Meeting Proceedings, CPIA Publ. 509, Vol. I, 1989, p. 357.

29. M. Esseghir and C.E. Polymeropoulos, *Combust. Flame* 73, 99 (1988).

30. D.A. Frank–Kamenetskii, "Diffusion and Heat Exchange in Chemical Kinetics," N. Thon, Translator, Princeton University Press, Princeton, 1955.

31. B.F. Gray and C.H. Yang, *J. Phys. Chem.* 69, 2747 (1965).

32. J.B. Fenn, *Ind. Engr. Chem.* 43, No. 12, 2865 (1951).

33. H.G. Adelman, in Eighteenth Symposium (International) on Combustion, The Combustion Institute, Pittsburgh, 1981, p. 1333.

34. M.T. Lim, R.W. Anderson and V.S. Arpaci, *Combust. Flame* 69, 303 (1987).

35. Y. Ko, V.S. Arpaci and R.W. Anderson, *Combust. Flame* 83, 88 (1991).

36. E. Sher and S. Refael, in Nineteenth Symposium (International) on Combustion, The Combustion Institute, Pittsburgh, 1982, p. 251.

37. S. Refael and E. Sher, *Combust. Flame* 59, 17 (1985).

38. E. Sher and J.C. Keck, *Combust. Flame* 66, 17 (1986).

39. J.A. Syage, R. Rianda, E.W. Fournier and R.B. Cohen, Twenty–Fourth JANNAF Combustion Subcommittee Meeting Proceedings, CPIA Publ. 476, Vol. I, 1987, p. 293.

40. S. Au, R. Haley and P.R. Smy, *Combust. Flame* 88, 50 (1992).

41. K. Ishii, T. Tsukamoto, Y. Ujiie and M. Kono, *Combust. Flame* 91, 153 (1992).

42. D. Bradley and F.K–K. Lung, *Combust. Flame* 69, 71 (1987).

43. D.R. Ballal and A.H. Lefebvre, *Proc. Roy. Soc. London A* 364, 277 (1978).

44. A.M. Danis, I. Namer and N.P. Cernansky, *Combust. Flame* 74, 285 (1988).

45. A.H. Lefebvre, A.M. Mellor and J.E. Peters, in "Alternative Hydrocarbon Fuels: Combustion and Chemical Kinetics," AIAA, New York, 1978, p. 138.

46. D.R. Ballal and A.H. Lefebvre, *Combust. Flame* 35, 155 (1979).

47. J.E. Peters and A.M. Mellor, *AIAA J. Energy* 6, 272 (1982).

48. D.L. Dietrich, N.P. Cernansky, A.M. Danis and I. Namer, *Combust. Sci. Tech.* 79, 325 (1991).

49. G. Li and C. Wang, *J. Electrostatics* 11, 319 (1982).

50. A. Mäki and K. Oy, Fifth Pyrotechnical Day, Pyroteknikdager 1977, Sektionen för Detonik och Förbäuning, Swedish National Defense Research Inst, 1977, p. 119.

51. F.W. Brown, D.J. Kinsler and F.C. Gibson, "Sensitivity of explosives to initiation by electrostatic discharges," Bur. Mines RI 5002, 1953.

52. A.M. Mellor, D.R. Stoops, T.P. Rudy and R.W. Hermsen, Workshop on ESD Ignition of Composite Solid Propellants Proceedings, Army Research Office, 1989, p. 133.

53. S. McHugh, "Solid mechanical deformation interactions with transient burning," Ninth International Conference on Mathematical and Computer Modeling, University of California at Berkeley, 1993.